Noninvasive Imaging of Osteoclasts in Parathyroid Hormone–Induced Osteolysis Using a ^{64}Cu-Labeled RGD Peptide

Jennifer E. Sprague[1], Hideki Kitaura[2], Wei Zou[2], Yunpeng Ye[1], Samuel Achilefu[1], Katherine N. Weilbaecher[3], Steven L. Teitelbaum[2], and Carolyn J. Anderson[1]

[1]Mallinckrodt Institute of Radiology, Washington University School of Medicine, St. Louis, Missouri; [2]Department of Pathology and Immunology, Washington University School of Medicine, St. Louis, Missouri; and [3]Department of Medicine, Washington University School of Medicine, St. Louis, Missouri

Bone diseases are often a result of increased numbers of osteoclasts, or bone-resorbing cells. Bone metastases are a significant cause of morbidity in many types of cancer. An imaging agent targeting osteoclasts, which are upregulated in osteolytic lesions, may facilitate earlier follow-up in patients with osteolytic or mixed bone metastases. Osteoclasts express high levels of $\alpha_v\beta_3$ integrin, to which peptides containing the Arg-Gly-Asp (RGD) sequence are known to bind. We proposed that radiolabeled RGD peptides could be used to detect osteoclasts in lytic bone lesions. **Methods:** The cross-bridged macrocyclic chelator 4,11-bis(carboxymethyl)-1,4,8,11-tetraazabicyclo[6.6.2]hexadecane (CB-TE2A) was conjugated to c(RGDyK) for radiolabeling with ^{64}Cu ($t_{1/2}$, 12.7 h; β^+, 17.4%; $E_{\beta+max}$, 656 keV; β^-, 39%; $E_{\beta-max}$, 573 keV). The in vitro affinity of Cu(II)-CB-TE2A-c(RGDyK) for $\alpha_v\beta_3$ and $\alpha_v\beta_5$ was evaluated in a heterologous competitive binding assay. Ex vivo uptake was examined in osteoclasts prepared from bone marrow macrophages. As a proof of principle, biodistribution and imaging studies were performed on parathyroid hormone (PTH)–induced osteolysis in the calvarium. **Results:** Cu-CB-TE2A-c(RGDyK) was shown to have a 30-fold higher affinity for $\alpha_v\beta_3$ than for $\alpha_v\beta_5$. Osteoclasts were shown to specifically take up ^{64}Cu-CB-TE2A-c(RGDyK). However, bone marrow macrophages showed only nonspecific uptake. PTH treatment increased calvarial uptake of ^{64}Cu-CB-TE2A-c(RGDyK), compared with uptake in mice receiving a sham treatment. In addition, calvarial uptake correlated linearly with the number of osteoclasts on the bone surface. **Conclusion:** These results suggest that ^{64}Cu-CB-TE2A-c(RGDyK) selectively binds $\alpha_v\beta_3$ on osteoclasts and may potentially be used to identify increased numbers of osteoclasts in osteolytic bone diseases such as osteolytic bone metastasis and inflammatory osteolysis.

Key Words: bone; PET/CT; radiopharmaceuticals; copper-64; integrin; osteoclast

J Nucl Med 2007; 48:311–318

Osteoclasts are multinucleated cells formed by the fusion of mononuclear progenitors of the monocyte/macrophage family. They are the principal cells involved in bone resorption. Bone diseases, both nonneoplastic and neoplastic, often involve increased numbers of osteoclasts. For example, the periarticular osteolysis that complicates rheumatoid arthritis is due to aggressive osteoclast recruitment.

The skeleton is one of the most common sites of cancer metastasis (*1*). It has been reported that in 75% of patients with metastatic breast cancer, metastatic bone lesions—which can be osteolytic, osteoblastic, or mixed—will develop (*2*). Breast cancer cells in bone stimulate recruitment of osteoclasts, resulting in osteolysis (*3*). Bone metastases cause significant morbidity, including pain, pathologic fracture, spinal cord compression, and hypercalcemia (*1,2*). In addition, microscopic bone tumor metastases appear to be an independent predictor of poor outcome in breast cancer even among lymph node–negative patients with primary tumors smaller than 2 cm (*4*).

The most common method for detecting bone metastases is γ-camera imaging using ^{99m}Tc-methylene diphosphonate (MDP), commonly referred to as a bone scan (*2*). Bone scans rely on osteoblast activity for incorporation of the ^{99m}Tc-MDP radiopharmaceutical into bone (*5*). Therefore, purely osteolytic lesions are poorly detectable (*6*), and bone tumors responding to anticancer therapy, with resultant bone healing involving osteoblast-mediated bone deposition, can exhibit a false-positive flare response for several months after treatment (*2,7,8*). PET with ^{18}F-FDG has been used for bone metastasis detection (*5*), but cells involved in inflammation and bone healing at metastatic foci may also have a high glucose uptake (*9,10*). Anatomic imaging methodologies such as radiography, MRI, and CT have also been used to detect or monitor bone metastases. However, metastases to the bone become apparent on radiographs only after the loss of more than 50% of the bone mineral content at the site of disease (*11*). The loss of bone density must be significant for CT to be able to detect

Received Aug. 16, 2006; revision accepted Nov. 3, 2006.
For correspondence or reprints contact: Carolyn J. Anderson, PhD, Mallinckrodt Institute of Radiology, Washington University School of Medicine, 510 S. Kingshighway Blvd., Campus Box 8225, St. Louis, MO 63110.
E-mail: andersoncj@wustl.edu

osteolytic bone lesions (*11*), and MRI detects tumor in the bone marrow but does not readily image bone degradation (*12*). Dual-energy x-ray absorptiometry scans are frequently used in osteoporosis to monitor changes in bone density and the response to antiresorptive therapy. These can be difficult to interpret in the case of compression fractures and osteoarthritis, which can occur in osteopenic populations. Therefore, imaging agents that identify osteoclasts in vivo are urgently needed to quantify the burden of osteolytic bone metastases, evaluate the response of osteolytic bone metastases to therapy, and identify which patients will respond to antiresorptive agents.

Cyclic pentapeptides containing an Arg-Gly-Asp (RGD) consensus sequence have been investigated as high-affinity $\alpha_v\beta_3$ ligands with good specificity (*13*). The integrin $\alpha_v\beta_3$ has increasingly become a target for tumor and angiogenesis imaging using radiolabeled RGD peptides (*14,15*). Osteoclasts express the highest levels of $\alpha_v\beta_3$ of any cell in the body (*16*), and $\alpha_v\beta_3$ ligands have been shown to inhibit osteoclast attachment to and absorption of bone (*17,18*). Therefore, $\alpha_v\beta_3$ integrin was selected as the target protein for osteoclast imaging in osteolytic bone disease.

Many tumor cells also express $\alpha_v\beta_3$ (*19*). For clinical imaging, detection of both tumor cells and associated osteoclasts would improve the sensitivity of an osteoclast-imaging agent targeting $\alpha_v\beta_3$. However, for validating an $\alpha_v\beta_3$ imaging agent for direct detection of osteoclasts, a model of pharmacologically induced osteolysis is appropriate to differentiate tumor cell–mediated and osteoclast-mediated uptake in bone lesions. Parathyroid hormone (PTH) induces osteoclast-mediated osteolysis when serially injected subcutaneously at the calvarium (*20*). This pharmacologic model of PTH-induced osteolysis will allow investigation of osteoclast-mediated bone uptake independent of tumor cells.

^{64}Cu ($t_{1/2}$, 12.7 h) is suitable for both PET and targeted radiotherapy because of its decay characteristics (β^+, 17.4%; $E_{\beta+max}$, 656 keV; β^-, 39%; $E_{\beta-max}$, 573 keV) (*21,22*) and because it can be produced at a high specific activity on a small biomedical cyclotron (*23*). Peptides and proteins are radiolabeled with ^{64}Cu using a covalently linked bifunctional chelator. Recent studies have shown that commonly used bifunctional chelators such as 1,4,7,10-tetraazacyclotetradecane-*N,N′,N″,N‴*-tetraacetic acid (DOTA) and 1,4,8,11-tetraazacyclotetradecane-1,4,8,11-tetraacetic acid (TETA) are unstable in vivo relative to the cross-bridged chelator 4,11-bis(carboxymethyl)-1,4,8,11-tetraazabicyclo[6.6.2]hexadecane (CB-TE2A) (*24*). Therefore, CB-TE2A is a better candidate for copper-based PET, resulting in lower liver and blood uptake and higher target-to-background signals than can be obtained with conventional bifunctional chelators (*25*).

Here, we have conjugated c(RGDyK) (*26*) to CB-TE2A for radiolabeling with ^{64}Cu (Fig. 1). Osteoclasts were shown to selectively take up ^{64}Cu-CB-TE2A-c(RGDyK) in vitro. In a proof-of-principle study, a mouse model of PTH-induced osteolysis was used to validate ^{64}Cu-CB-TE2A-c(RGDyK) for osteoclast imaging in vivo.

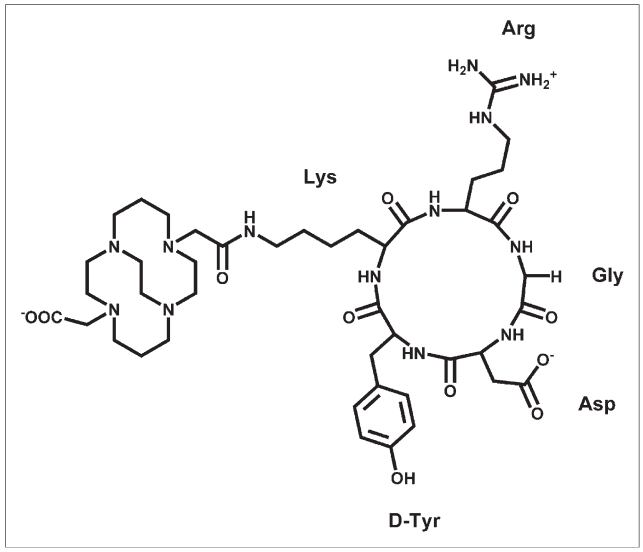

FIGURE 1. Structure of CB-TE2A-c(RGDyK).

MATERIALS AND METHODS

^{64}Cu was produced on a CS-15 biomedical cyclotron at Washington University School of Medicine according to published procedures (*23*). Copper chloride ($CuCl_2$) was purchased from Johnson Matthey. Fmoc–amino acid building blocks, 2-(1*H*-benzotriazole-1-yl)-1,1,3,3-tetramethyluronium hexafluorophosphate, and *N*-hydroxybenzotriazole were purchased from AnaSpec. Trifluoroacetic acid (TFA) was purchased from Advanced ChemTech. All other chemicals were purchased from Sigma-Aldrich Chemical Co. All solutions were prepared using ultrapure water (resistivity, 18 MΩ-cm). Radio-thin-layer chromatography (radio-TLC) was performed using $MKC_{18}F$ reversed-phase plates (Whatman), with 10% ammonium acetate:methanol (30:70) as the mobile phase. Radio-TLC detection was accomplished using an AR2000 imaging scanner (Bioscan). Analytical reversed-phase high-performance liquid chromatography (HPLC) was performed on a 600E chromatography system (Waters) with a 996 photodiode array detector (Waters) and a model 661 radioactivity detector (EG&G Ortec). Radioactive samples were counted using an 8000 automated well-type γ-counter (Beckman). Electrospray mass spectrometry was accomplished using a Micromass ZQ (Waters). Male C57BL/6 mice (8 wk old) were purchased from Charles River Laboratories.

Synthesis of CB-TE2A-c(RGDyK)

The cyclic peptide was prepared in 3 steps consisting of solid-phase peptide synthesis, intramolecular cyclization in solution, and conjugation of peptide with CB-TE2A, as described previously (*27*). Briefly, the orthogonally protected linear peptide [DTyr(Bu^t)-Lys(Dde)-Arg(Pbf)-Gly-Asp(OBu^t)-O-resin] was prepared on a 2-chlorotrityl resin (0.62 g, 0.64 mmol/g) and cleaved with 1% TFA in dichloromethane. After cyclizing the protected peptide in a solution of PyBOP (2.5 equivalents), *N*-hydroxybenzotriazole (2.5 equivalents), and diisopropylethylamine (5 equivalents)

in *N,N*-dimethylformamide/dichloromethane (1:10 v/v), the Dde group was selectively removed with 1% hydrazine in methanol. CB-TE2A (3 equivalents) was conjugated to the free ε-amino lysine group of the peptide (1 equivalent) in the presence of diisopropylcarbodiimide (10 equivalents), and *N*-hydroxybenzotriazole (3 equivalents) in anhydrous *N,N*-dimethylformamide. All side-chain–protecting groups were removed with 95% aqueous TFA solution, and the crude product was purified by HPLC (9.6 mg, ~8% yield) and identified by electrospray mass spectrometry. The observed m/z for $[MH]^+$ and $[MH_2]^{2+}$ in electrospray mass spectrometry was 944.37 and 472.77, respectively. Additional unconjugated c(RGDyK) for integrin-binding assays and blocking studies in mice was purchased from CS Bio.

Radiolabeling with ^{64}Cu

CB-TE2A-c(RGDyK) was radiolabeled with ^{64}Cu according to the method previously described for radiolabeling a CB-TE2A-peptide conjugate (*25*). Briefly, $^{64}CuCl_2$ was added to CB-TE2A-c(RGDyK) in 0.1-M NH_4OAc, pH 8, and heated for 45–60 min. Radiochemical purity was assessed by radio-HPLC (99% A to 70% A in 15 min, 1 mL/min; A = 0.1% TFA in H_2O, B = 0.1% TFA in acetonitrile; C-18 monomeric column [Vydac], 3 μm, 4.6 × 100 mm) or radio-TLC. Specific activity and radiochemical purity were calculated on the basis of both radio-HPLC and radio-TLC. Because these yielded similar results, the presented values represent only radio-TLC data. High radiochemical purity (>95%) and specific activity (≤103.6 MBq/μg [2.8 mCi/μg]) were achieved. Identical conditions were used for ^{nat}Cu(II) labeling. Formation of the correct complex was demonstrated by HPLC and mass spectrometry ($C_{43}H_{67}N_{13}O_{11}Cu$ $(M+H)^+$; calculated m/z, 1005.45; measured m/z, 1005.21).

Integrin-Binding Assays

The affinity of each peptide for $\alpha_v\beta_3$ and $\alpha_v\beta_5$ integrins was estimated using the method described previously by Haubner et al. (*28*). Briefly, vitronectin (Chemicon) (630 μg/mL) was biotinylated with *N*-hydroxysuccinimide biotin (1.27 μg/mL; 2 h at room temperature) before dialysis into phosphate-buffered saline, pH 7.4. $\alpha_v\beta_3$ or $\alpha_v\beta_5$ (EMD Bioscience) (1 μg/mL) in coating buffer (20-mM Tris, pH 7.4, 150-mM NaCl, 2-mM $CaCl_2$, 1-mM $MgCl_2$, 1-mM $MnCl_2$) was coated onto 96-well plates (Nunc Immuno Plate with MaxiSorp) (1 h at 4°C). The plates were then blocked (1 h at 4°C) with bovine serum albumin (3% in coating buffer). After washing twice with binding buffer (0.1% bovine serum albumin in coating buffer), biotinylated vitronectin (14 nM) with and without serially diluted peptides was allowed to bind to the integrins (3 h at 37°C). After washing (3 times in binding buffer), bound biotinylated vitronectin was detected by binding ExtrAvidin alkaline phosphatase (Sigma) (1/35,000 dilution, 1 h at room temperature) using the *p*-nitrophenyl phosphate liquid substrate system (Sigma) as the chromogen. Each concentration data point was done in triplicate, and each binding experiment was performed at least twice. Nonlinear regression was used to fit binding curves and calculate inhibitory concentrations of 50% (IC_{50} values) (Prism, version 4.0; GraphPad).

Preparation of Osteoclasts and Macrophages from Bone Marrow

Bone marrow macrophages (BMMs) ($\alpha_v\beta_5$-positive) were isolated and induced to differentiate into osteoclasts ($\alpha_v\beta_3$-positive) according to previously described methods (*29*). Briefly, 8-wk-old male C57BL/6 mice were sacrificed by cervical dislocation. Femurs and tibias were removed aseptically. Both ends of bones were cut off using scissors, and bone marrow was flushed out by injecting α–minimal essential medium (MEM) into one end with a sterile needle. Cell clumps were dispersed by pipetting, and large debris was removed by passage through a 70-μm cell strainer. Cells were pelleted, washed once with α-MEM, and resuspended in α-MEM plus 10% heat-inactivated (Δ) fetal bovine serum (Hyclone Defined; Fisher Scientific). BMMs were grown at 37°C in a humidified 5% CO_2 atmosphere in α-MEM, 10% Δ fetal bovine serum, and a 1/10 volume of CMG14-12 culture supernatant (macrophage colony-stimulating factor [M-CSF], 100 ng/mL), in 10-cm suspension culture dishes (5 plates per mouse). After 3 d in culture, the dishes were washed twice with phosphate-buffered saline, and the cells were harvested by pipetting in 0.02% ethylenediaminetetraacetic acid. The cells were plated in 6-well plates at 150,000 cells per well. Macrophages were maintained under the conditions described above. Osteoclast differentiation was induced by the addition of 100 ng of receptor activator of NF-κB ligand (RANKL) per milliliter (*30*). After 4 additional days in culture, large multinucleated cells were clearly visible in the osteoclast wells.

To demonstrate osteoclast differentiation, we stained the cells for tartrate-resistant acid phosphatase (TRAP). The cells were fixed for 2 h at room temperature in 10% formalin. Fixed cells were washed (2 times in phosphate-buffered saline) and incubated for 1 h at room temperature in 0.2% Triton X-100. After washing, the cells were incubated for 5–20 min in 100-mM sodium acetate, pH 5.0, containing 50-mM sodium tartaric acid, 1.3-mM fast red violet salt, and 0.3-mM naphthol AS-MX phosphate (3-hydroxy-2-naphthoic acid 2,4-dimethylanilide).

In Vitro Cell Uptake

The procedure for the cellular uptake assay was based on the method published by Wang et al. (*31*). Osteoclasts and macrophages were prepared as described above. The cells were washed twice with Hank's balanced salt solution, and then 1 mL of fresh α-MEM plus 10% Δ fetal bovine serum was added to each well. To demonstrate specific uptake, c(RGDyK) (0–4,000 nM) was added to each well. To each well was added ^{64}Cu-CB-TE2A-c(RGDyK) (specific activity, 20.0 MBq/μg [0.54 mCi/μg]) to a final concentration of 4.0 nM. The cells were incubated for 2 h at 37°C in a humidified 5% CO_2 atmosphere. The cells were then lysed by the addition of 100 μL of 2% sodium dodecylsulfate; cell lysate was removed using a cell scraper to pool the lysate and pipetted into a clean microcentrifuge tube. Lysates were sonicated 15 s and then heated for 5 min at 95°C to denature all proteins. Cell uptake was measured by counting each lysate in a γ-counter. The total protein concentration in each lysate was determined using the bicinchoninic acid protein assay (Pierce Biotechnology). Uptake was expressed as femtomoles of radiotracer per milligram of protein.

Western Blot Analysis

Cell lysate proteins were resolved on 7.5% Tris-HCl Ready Gel (BioRad Laboratories) under denaturing, reducing conditions. $\alpha_v\beta_3$ and $\alpha_v\beta_5$ integrin standards (Chemicon) were also run. Proteins were transferred to a polyvinyl diisopropyl fluoride membrane, and membranes were blocked in 5% nonfat dry milk in Tris-buffered saline 0.1% TWEEN 20 (TBST). Membranes were incubated overnight at 4°C in primary antibody (anti-β_3 integrin antibody [Cell Signaling] or anti-β_5 integrin antibody [Chemicon]) in 5% bovine serum albumin in TBST. Membranes were washed (3 times for 5 min each) in TBST and then incubated for 1 h at

room temperature in horseradish peroxidase conjugated goat anti-rabbit IgG (Cell Signaling) in 5% milk in TBST. After washing (3 times for 5 min each) in TBST, blots were developed using ECL western blotting detection reagents (Amersham Biosciences Corp.).

Biodistribution and Small-Animal PET of Induced Osteoclastogenesis

All animal experiments were performed in compliance with the Guidelines for the Care and Use of Research Animals established by the Animal Studies Committee of Washington University. For induction of osteoclastogenesis in vivo, 10 μg of PTH (1-34 human; Bachem Bioscience Inc.) were injected subcutaneously at the calvarium every 6 h for 4 d (*20*). The mice were used 6 h after the last treatment.

After treatment, the mice received ^{64}Cu-CB-TE2A-c(RGDyK) (0.74 MBq [20 μCi] for biodistribution; 5.6–11.1 MBq [150–300 μCi] for small-animal PET) via tail vein injection. In blocking studies, 18 mg of c(RGDyK) (CS Bio Co.) per kilogram were coinjected. For biodistribution, the mice were sacrificed at 1 h after injection, and organs of interest were harvested, weighed, and counted on a γ-counter. Calvaria were weighed and then placed in 10% formalin for fixing before counting. PET was performed on a small-animal PET scanner (microPET Focus 120 or 220; Siemens Medical Solutions). Mice anesthetized with 1%–2% isoflurane were imaged for 10 min at 1 h after tail vein injection of ^{64}Cu-CB-TE2A-c(RGDyK). Coregistration of the small-animal PET images was achieved in combination with a microCAT-II small-animal CT camera (Imtek Inc.) (15-min image acquisition), which provides high-resolution CT anatomic images. Registration between small-animal CT and PET images was accomplished by a landmark registration technique with image display software (AMIRA; TGS Inc.). The registration method proceeds by rigid transformation of the small-animal CT images from landmarks provided by fiducial markers attached directly to the animal bed. Maximum a posteriori (MAP) reconstruction was used for the PET component of the coregistered images (*32*). Regions of interest were drawn on coregistered small-animal CT images, and region-of-interest activity on corresponding small-animal PET images was measured using AMIRA software. These values were converted to standardized uptake values (SUVs) using the formula (nCi/mL) × (animal weight [g]/injected dose [nCi]). After imaging, the mice were sacrificed for post-PET biodistribution analysis as described above.

After 1 wk had been allowed for radioactive decay, the calvaria were decalcified for 24 h in 14% ethylenediaminetetraacetic acid. Histologic analysis was performed according to previously described methods (*30*).

Statistics

All data are presented as mean ± SD. For statistical classification, 1-way ANOVA with a Bonferroni posttest was used to determine statistically significant differences between the control, PTH, and PTH-plus-block groups. A Student *t* test (2-tailed, unpaired) was used to compare individual datasets. All statistical analysis was performed using PRISM software (GraphPad). *P* values less than 0.05 were considered significant.

RESULTS

In Vitro Affinity Assay

The effect of conjugation of c(RGDyK) to CB-TE2A on integrin-binding affinity was assessed. The affinities of c(RGDyK) and Cu(II)-CB-TE2A-c(RGDyK) for $\alpha_v\beta_3$ and $\alpha_v\beta_5$ integrins were determined using a heterologous competitive-binding assay with biotinylated vitronectin, recognized by both integrins, as the competing ligand. Conjugation of Cu(II)-CB-TE2A to c(RGDyK) peptide did not significantly alter peptide affinity (Table 1). Replicate experiments produced IC_{50} values within the same confidence intervals. In addition, these data demonstrate an approximately 30-fold higher binding affinity for $\alpha_v\beta_3$ than for $\alpha_v\beta_5$ in vitro.

Ex Vivo Cell Uptake

To validate selective targeting of ^{64}Cu-CB-TE2A-c(RGDyK) to $\alpha_v\beta_3$-positive cells, we examined ex vivo cell uptake by BMMs (Fig. 2A) and osteoclasts (Fig. 2C). Two hours after the addition of ^{64}Cu-CB-TE2A-c(RGDyK) to the cell culture medium, cell uptake was measured (Fig. 2B). Uptake of ^{64}Cu-CB-TE2A-c(RGDyK) by osteoclasts was selectively blocked by increasing concentrations of c(RGDyK). Nonlinear regression analysis of the osteoclast dose–activity curve yielded an IC_{50} value of 155 nM, a lower affinity than that measured for binding to isolated $\alpha_v\beta_3$ integrin (IC_{50}, 6 nM).

Osteoclast uptake of ^{64}Cu-CB-TE2A-c(RGDyK) in the absence of competing c(RGDyK) was 2.6 ± 0.7–fold higher than BMM uptake under the same conditions. In addition, BMM uptake was not blocked by c(RGDyK), thus suggesting that the low-level BMM uptake is nonspecific. The presence of β_3 integrin in osteoclasts and the absence in macrophages were confirmed by Western blot of cell lysates after each uptake experiment (Fig. 2D).

Detection of Pharmacologically Induced Osteoclastogenesis In Vivo

To examine osteoclast-mediated bone uptake in vivo in the absence of tumor cells, we used a model of pharmacologically induced osteolysis. PTH was serially injected

TABLE 1
Affinity of c(RGDyK) and Cu(II)-CB-TE2A-c(RGDyK) for Integrins $\alpha_v\beta_3$ and $\alpha_v\beta_5$ as Determined in Heterologous Competitive Binding Assay Using Biotinylated Vitronectin

Compound	$\alpha_v\beta_3$		$\alpha_v\beta_5$	
	IC_{50} (nM)	95% confidence interval	IC_{50} (nM)	95% confidence interval
Cu(II)-CBTE2A-c(RGDyK)	6.0	3.7–9.6	171	110–266
c(RGDyK)	3.7	2.7–5.0	194	142–266

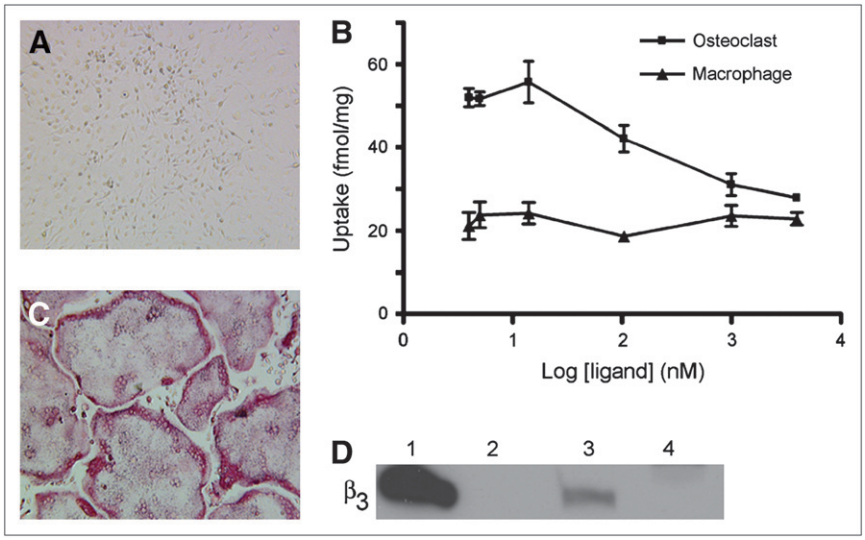

FIGURE 2. Uptake of ^{64}Cu-CB-TE2A-c(RGDyK) by osteoclasts and macrophages. BMMs were harvested from mice and grown in culture. (A) Cells treated with only M-CSF remained TRAP(−) mononuclear macrophages. (C) Cells cultured in presence of MCSF plus RANKL differentiated into large, TRAP(+) osteoclasts (red stain). (B) Cell uptake was determined 2 h after addition of ^{64}Cu-CB-TE2A-c(RGDyK) (4 nM) plus c(RGDyK) (0–4,000 nM) to medium of cells grown in 6-well plates. Each data point represents average of triplicate measurements. (D) Integrin expression was evaluated by Western blot against β_3. Lanes: 1 = $\alpha_v\beta_3$ standard, 10 ng; 2 = empty; 3 = osteoclast lysate, 20 μg; 4 = macrophage lysate, 20 μg.

subcutaneously at the calvarium every 6 h for 4 d. This procedure resulted in localized osteoclastogenesis and concurrent bone loss in the calvarium as determined by histologic examination (Figs. 3A and 3D). Biodistribution studies (1 h after injection of ^{64}Cu-CB-TE2A-c(RGDyK)) were performed on control and PTH-treated mice ($n = 4$ per group) and were repeated on control mice and mice treated with PTH with or without an 18 mg/kg blocking dose of c(RGDyK) ($n = 4$ per group). Data from control and PTH groups from each experiment were pooled for final analysis (Fig. 3B). Comparison of control and PTH-treated mice revealed a 1.9-fold increase in calvarial uptake ($P < 0.0001$) without a concomitant increase in non-targeted organ uptake. In particular, we noted no increase in scalp uptake in PTH-treated mice relative to scalp uptake in controls; thus, any calvarial uptake visible on small-animal PET can be attributed to bone rather than to soft tissue. The calvarium-to-blood ratio was significantly increased in PTH-treated mice (4.6 ± 1.3), compared with controls (2.3 ± 0.7) ($P = 0.0005$).

Treatment with 18 mg of c(RGDyK) per kilogram resulted in reduced uptake in all dissected tissues, excluding blood (Fig. 3B). Blocking was most pronounced in the calvarium, femur, and spleen (>80% block) relative to uptake in PTH-treated mice. The calvarium-to-blood and calvarium-to-muscle uptake ratios were significantly reduced in PTH-plus-block mice (blood, 1.1 ± 0.3; muscle, 2.8 ± 0.6) relative to PTH mice (blood, 4.6 ± 1.3; muscle, 4.6 ± 0.9) ($P < 0.001$). No statistically significant difference in calvarium-to-blood or calvarium-to-muscle uptake ratios was found between control mice (blood, 2.3 ± 0.7; muscle, 1.9 ± 0.2) and PTH-plus-block mice ($P > 0.05$).

Because PTH treatment appears to increase calvarial uptake of ^{64}Cu-CB-TE2A-c(RGDyK), we next sought to determine whether a correlation could be made between uptake and osteoclast number. The percentage of skull

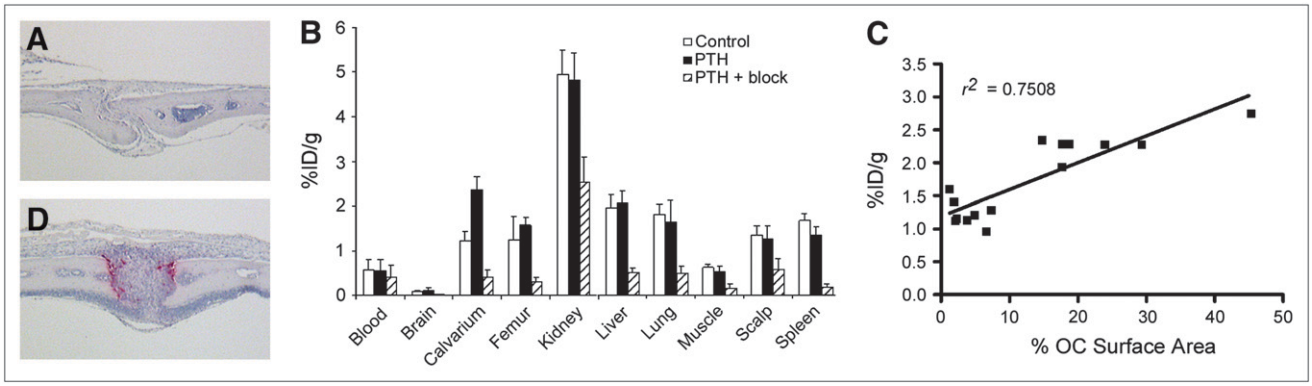

FIGURE 3. PTH induces osteoclasts resulting in increased uptake of ^{64}Cu-CB-TE2A-c(RGDyK) at calvarium. TRAP-stained sections of calvarium of control mice (A) and PTH-treated mice (D) confirm osteoclast induction after PTH treatment. Osteoclasts stain red. (B) Biodistribution (1 h after injection) was performed on control mice ($n = 8$), PTH-treated mice ($n = 8$), and PTH-plus-block mice injected with 740 kBq (20 μCi) (10.5–12 ng) of ^{64}Cu-CB-TE2A-c(RGDyK). Note that $n = 7$ for PTH femur because of contamination of 1 sample by urine. (C) Uptake of ^{64}Cu-CB-TE2A-c(RGDyK) (biodistribution 1 h after injection: control, $n = 7$; PTH, $n = 7$) was plotted against ratio of osteoclast surface area to total surface area.

suture surface area covered by osteoclasts relative to total surface area was determined histomorphometrically for mice in both biodistribution studies. A linear correlation (Pearson correlation, 2-tailed) between percentage osteoclast surface area and percentage injected dose per gram was obtained (Fig. 3C) ($r^2 = 0.7508$, $P < 0.0001$). Thus, as the number of osteoclasts on bone increased, uptake of ^{64}Cu-CB-TE2A-c(RGDyK) by that bone also increased, suggesting osteoclast-specific uptake in bone.

Small-animal PET with small-animal CT coregistration was performed on control mice ($n = 2$), PTH mice ($n = 4$), and PTH-plus-block mice ($n = 2$) simultaneously with biodistribution studies. MAP reconstruction was used to maximize image resolution given the thinness of the bone at the calvarium. The images shown (Fig. 4) are representative of all mice in each group. In both transaxial and sagittal sections, increased uptake at the calvarium is clearly evident in the PTH mouse relative to the control mouse and the PTH-plus-block mouse. SUVs calculated for PTH-treated mice (0.40 ± 0.10, $n = 4$) were significantly higher than those for control mice (0.19 ± 0.03, $n = 2$) or PTH-plus-block mice (0.18 ± 0.01, $n = 2$) ($P = 0.0291$, 1-way ANOVA, Bonferroni multiple-comparison test). SUVs did not differ between control mice and PTH-plus-block mice. In all groups, a region of high radiotracer uptake was noted at the base of the teeth. Uptake in this region was reduced in the PTH-plus-block mice relative to the PTH mice. Tooth uptake may be $\alpha_v\beta_3$ integrin–specific for osteoclasts, as the teeth grow throughout a rodent's lifetime (*33*), thus producing continual bone remodeling at this site.

DISCUSSION

The goal of this study was to determine whether the $\alpha_v\beta_3$ integrin is a potential imaging biomarker for the presence of increased numbers of osteoclasts, which are implicated in bone diseases such as inflammatory osteolysis and osteolytic bone metastases. Osteoclasts are known to have high concentrations of the $\alpha_v\beta_3$ integrin, and bone resorption can be blocked by blocking $\alpha_v\beta_3$ function (*16*). To show a proof of principle, we set out to determine whether the PET agent ^{64}Cu-CB-TE2A-c(RGDyK) is taken up specifically by osteoclasts and whether pharmacologically induced osteolysis is specifically imaged using this agent.

The group of Chen et al. has previously reported an RGD peptide monomer, a dimer, and a tetramer, each conjugated to the chelator DOTA for radiolabeling with ^{64}Cu (*34–36*). However, on the basis of previous studies, ^{64}Cu-CB-TE2A-c(RGDyK) was expected to show improved liver clearance, compared with that of ^{64}Cu-DOTA-c(RGDyK) (*24,25*). Because biodistribution showed that PTH treatment had no effect on liver uptake, post-PET data from control and PTH-treated mice were averaged in order to increase sample size. Post-PET liver uptake (1.52 ± 0.13 [$n = 5$]) decreased by 22% and 27% relative to that in 1-h biodistribution control and PTH mice, respectively ($P = 0.001$). In contrast, liver uptake did not decrease significantly between 1 and 4 h after injection for ^{64}Cu-DOTA-c(RGDyK) ($P = 0.34$) (*34*). These data further validate CB-TE2A as a bifunctional Cu(II) chelator superior to DOTA.

Cell uptake studies clearly demonstrated specific uptake of ^{64}Cu-CB-TE2A-c(RGDyK) by osteoclasts but not BMMs. Interestingly, the calculated affinity of ^{64}Cu-CB-TE2A-c(RGDyK) was significantly lower for isolated $\alpha_v\beta_3$ than for integrin on the surface of osteoclasts in culture. $\alpha_v\beta_3$ can transition between an active and a basal conformational state with a different ligand in the osteoclast (*37*). Clustering of $\alpha\beta$ heterodimers also modulates ligand binding (*38*). We propose that the activation state of a purified integrin may be

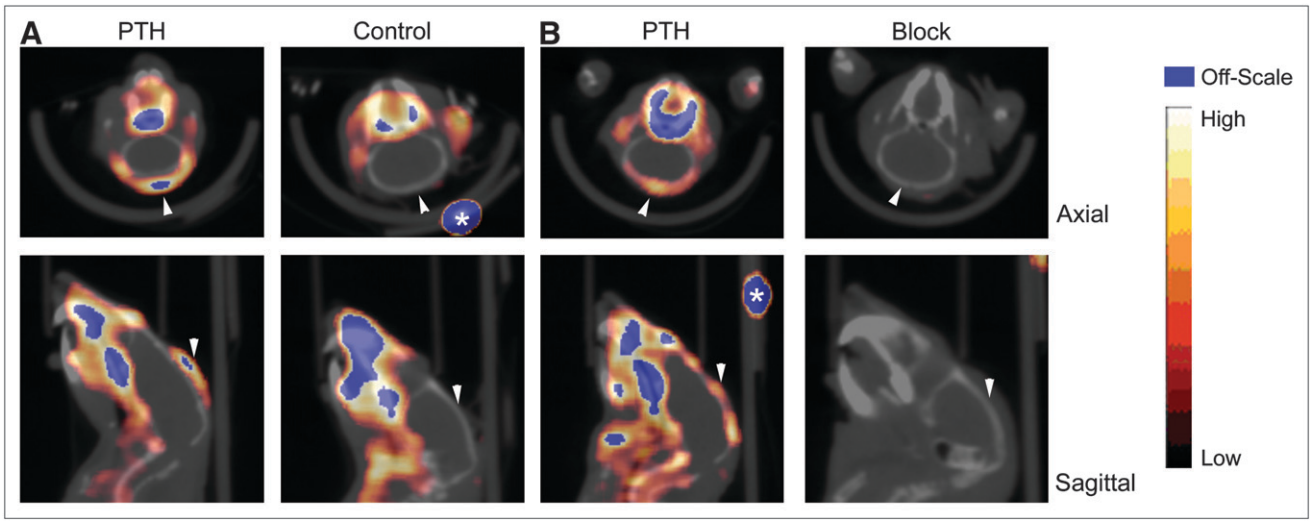

FIGURE 4. Small-animal PET/CT of PTH-treated mice. Calvarium uptake of ^{64}Cu-CB-TE2A-c(RGDyK) was higher in PTH-treated mice (7.4 MBq [199 μCi],115 ng, SUV = 0.53) than in control mice (7.7 MBq [209 μCi], 121 ng, SUV = 0.22) (50- to 60-min summed dynamic image) (A). In PTH-treated mice, uptake was reduced in all tissues, including calvarium, after injection of c(RGDyK) (PTH [left]: 159 μCi, 84 ng, SUV = 0.33; block [right]: 164 μCi, 87 ng, SUV = 0.18) (static image obtained 60 min after injection, 10-min scan) (B). Arrowheads indicate calvarium of each animal. Fiducials (*) are indicated.

different from that of an integrin on an intact cell membrane in culture. Consistent with our ex vivo data, studies of related peptides have shown inhibition of tumor cell or osteoclast adhesion to vitronectin- or serum-coated surfaces, with IC_{50} values in the low micromolar range (*39*).

We observed a 2.6-fold increase in maximal osteoclast uptake, compared with nonspecific BMM uptake. This relatively low level of specific uptake by osteoclasts in culture would not support ^{64}Cu-CB-TE2A-c(RGDyK) as an agent able to detect osteoclasts in vivo. However, increased uptake at the site of induced osteolysis was clearly visible on small-animal PET. In addition, the region of highest uptake within the calvarium on PET/CT appeared to correlate with the sagittal suture, where the highest number of osteoclasts were noted on histology. To the best of our knowledge, no quantitative measurements of RGD-binding sites (B_{max}) on osteoclasts in culture or in vivo have been previously reported. Therefore, higher numbers of in vivo binding sites or higher-affinity binding sites on activated osteoclasts cannot be ruled out.

Biodistribution studies demonstrated a significant increase in calvarium uptake in PTH-treated mice relative to controls. PTH did not appear to increase ^{64}Cu-CB-TE2A-c(RGDyK) uptake in tissues other than the calvarium. However, blocking with c(RGDyK) resulted in reduced uptake in all tissues examined. Similar multiorgan blocking has been reported for a related tetrameric RGD peptide in a tumor xenograft model (*35*). It is well known that RGD peptides do show low-level affinity for other integrins (*15*). Therefore, blocking studies do not appear well suited to demonstrating binding specificity for RGD peptides. Interestingly, the greatest degree of blocking was observed in the target tissues calvarium and femur—as would be predicted on the basis of the presence of osteoclasts—as well as in the spleen, the site of high levels of $\alpha_v\beta_5$-positive macrophages. Still, we did observe a significant correlation between bone surface area covered by osteoclasts and ^{64}Cu-CB-TE2A-c(RGDyK) uptake in the calvarium, thus suggesting osteoclast-specific uptake in bone. This relationship was likely reduced in our study because we examined whole calvarium uptake despite the fact that only a small portion of the calvarium was composed of osteoclasts.

The ability to noninvasively detect osteoclasts could have a significant impact on the clinical management of bone metastases by facilitating earlier detection of new lesions and potentially earlier follow-up of treatment response. In addition, imaging osteoclasts might allow clinicians to predict which patients would be responsive to treatment with bisphosphonates, a mainstay in bone metastasis therapy.

Beyond utility in managing neoplastic disease, osteoclast imaging could also find a use in several nonneoplastic bone diseases. For example, osteoporosis, which affects a large proportion of Western postmenopausal women, occurs when osteoclast-mediated bone resorption exceeds bone formation, and antiosteoporosis therapy typically targets osteoclasts (*40*). Disease progression is monitored by measuring bone density over a period of years using dual-energy x-ray absorptiometry (*40*). Osteoclast imaging might allow early follow-up after treatment initiation to determine whether the dose should be increased or an alternative therapy should be tried.

Periarticular osteolysis, a crippling complication of rheumatoid arthritis, is also caused by exuberant osteoclast recruitment (*41*). Early imaging of the joints of rheumatoid patients may allow selection of those prone to the development of bone destruction. The relevance of this approach is underscored by the fact that although anticytokine therapy is effective in arresting periarticular osteolysis, the therapy is not without risk. Thus, identifying individuals with early, clinically undetectable joint destruction would be of value.

These studies strongly support specific uptake of ^{64}Cu-CB-TE2A-c(RGDyK) by osteoclasts both ex vivo and in vivo. This osteoclast-mediated uptake was visualized on small-animal PET images of pharmacologically induced osteolysis, validating ^{64}Cu-CB-TE2A-c(RGDyK) uptake in a lytic bone lesion independent of tumor cells. Although some tumor cells do express $\alpha_v\beta_3$, we propose that imaging tumor cells in conjunction with osteoclasts would improve sensitivity for early detection, though it might reduce utility in predicting the bone metastasis response to bisphosphonates. Additionally, $\alpha_v\beta_3$ ligands of higher affinity, such as CB-TE2A–conjugated dimers or tetramers of c(RGDyK), will undoubtedly improve specific uptake in osteoclasts, compared with that obtained with the c(RGDyK) monomer. Future studies will address these questions by imaging osteoclasts in animal models of bone metastasis.

ACKNOWLEDGMENTS

We thank Angela Hirbe and Joseph Ippolito for helpful suggestions, and we acknowledge Dr. Gary R. Weisman at the University of New Hampshire for providing the chelator CB-TE2A; Todd A. Perkins, Thomas Voller, and Deborah Sultan for producing the ^{64}Cu; and Laura Meyer, Christopher Sherman, Nicole Fettig, Margaret Morris, Terry Sharp, and Lori Strong for providing excellent technical assistance. This research was supported by NCI grants R21 CA098698, AR03278, AR046523, AR048853, and P30 CA91842 (Alvin J. Siteman Cancer Center at Washington University in St. Louis). The production of ^{64}Cu at Washington University School of Medicine was supported by NCI grant R24 CA86307, and the small-animal imaging studies were supported by NCI R24 CA83060 (Washington University Small Animal Imaging Resource) and NCI P30 CA91842 (Siteman Cancer Center). One of the authors was supported by grant W81XWH-04-1-0396 from the Department of Defense Breast Cancer Research Program.

REFERENCES

1. Kakonen SM, Mundy GR. Mechanisms of osteolytic bone metastases in breast carcinoma. *Cancer.* 2003;97:834–839.
2. Hamaoka T, Madewell JE, Podoloff DA, Hortobagyi GN, Ueno NT. Bone imaging in metastatic breast cancer. *J Clin Oncol.* 2004;22:2942–2953.

3. Mundy GR. Metastasis to bone: causes, consequences and therapeutic opportunities. *Nat Rev Cancer.* 2002;2:584–593.
4. Braun S, Vogl FD, Naume B, et al. A pooled analysis of bone marrow micrometastasis in breast cancer. *N Engl J Med.* 2005;353:793–802.
5. Peterson JJ, Kransdorf MJ, O'Connor MI. Diagnosis of occult bone metastases: positron emission tomography. *Clin Orthop Relat Res.* 2003;415(suppl):S120–S128.
6. Roodman GD. Mechanisms of bone lesions in multiple myeloma and lymphoma. *Cancer.* 1997;80:1557–1563.
7. Schneider JA, Divgi CR, Scott AM, et al. Flare on bone scintigraphy following Taxol chemotherapy for metastatic breast cancer. *J Nucl Med.* 1994;35: 1748–1752.
8. Janicek MJ, Hayes DF, Kaplan WD. Healing flare in skeletal metastases from breast cancer. *Radiology.* 1994;192:201–204.
9. Mortimer JE, Dehdashti F, Siegel BA, Trinkaus K, Katzenellenbogen JA, Welch MJ. Metabolic flare: indicator of hormone responsiveness in advanced breast cancer. *J Clin Oncol.* 2001;19:2797–2803.
10. Dehdashti F, Flanagan FL, Mortimer JE, Katzenellenbogen JA, Welch MJ, Siegel BA. Positron emission tomographic assessment of "metabolic flare" to predict response of metastatic breast cancer to antiestrogen therapy. *Eur J Nucl Med Mol Imaging.* 1999;26:51–56.
11. Eustace S, Tello R, DeCarvalho V, et al. A comparison of whole-body turboSTIR MR imaging and planar ^{99m}Tc-methylene diphosphonate scintigraphy in the examination of patients with suspected skeletal metastases. *AJR.* 1997;169:1655–1661.
12. Mouchess ML, Sohara Y, Nelson MD Jr, DeClerck YA, Moats RA. Multimodal imaging analysis of tumor progression and bone resorption in a murine cancer model. *J Comput Assist Tomogr.* 2006;30:525–534.
13. Burgess K, Lim D, Mousa SA. Synthesis and solution conformation of cyclo[RGDRGD]: a cyclic peptide with selectivity for the alpha V beta 3 receptor. *J Med Chem.* 1996;39:4520–4526.
14. Haubner R, Weber WA, Beer AJ, et al. Noninvasive visualization of the activated alphavbeta3 integrin in cancer patients by positron emission tomography and [^{18}F]galacto-RGD. *PLoS Med.* 2005;2:e70.
15. Haubner R, Wester H-J, Burkhar F, et al. Glycosylated RDG-containing peptides: tracer for tumor targeting and angiogenesis imaging with improved biokinetics. *J Nucl Med.* 2001;42:326–336.
16. Horton MA. The alpha v beta 3 integrin "vitronectin receptor". *Int J Biochem Cell Biol.* 1997;29:721–725.
17. Fisher JE, Caulfield MP, Sato M, et al. Inhibition of osteoclastic bone resorption in vivo by echistatin, an "arginyl-glycyl-aspartyl" (RGD)-containing protein. *Endocrinology.* 1993;132:1411–1413.
18. Crippes BA, Engleman VW, Settle SL, et al. Antibody to beta3 integrin inhibits osteoclast-mediated bone resorption in the thyroparathyroidectomized rat. *Endocrinology.* 1996;137:918–924.
19. Felding-Habermann B. Integrin adhesion receptors in tumor metastasis. *Clin Exp Metastasis.* 2003;20:203–213.
20. Yates AJ, Gutierrez GE, Smolens P, et al. Effects of a synthetic peptide of a parathyroid hormone-related protein on calcium homeostasis, renal tubular calcium reabsorption, and bone metabolism in vivo and in vitro in rodents. *J Clin Invest.* 1988;81:932–938.
21. Lewis JS, Srinivasan A, Schmidt MA, Anderson CJ. In vitro and in vivo evaluation of ^{64}Cu-TETA-Tyr3-octreotate: a new somatostatin analog with improved target tissue uptake. *Nucl Med Biol.* 1999;26:267–273.
22. Connett JM, Anderson CJ, Guo LW, et al. Radioimmunotherapy with a Cu-64-labeled monoclonal antibody: a comparison with Cu-67. *Proc Natl Acad Sci U S A.* 1996;93:6814–6818.
23. McCarthy DW, Shefer RE, Klinkowstein RE, et al. Efficient production of high specific activity Cu-64 using a biomedical cyclotron. *Nucl Med Biol.* 1997;24: 35–43.
24. Boswell CA, Sun X, Niu W, et al. Comparative *in vivo* stability of copper-64-labeled cross-bridged and conventional tetraazamacrocyclic complexes. *J Med Chem.* 2004;47:1465–1474.
25. Sprague JE, Peng Y, Sun X, et al. Preparation and biological evaluation of copper-64-Tyr^3-octreotate using a cross-bridged macrocyclic chelator. *Clin Cancer Res.* 2004;10:8674–8682.
26. Haubner R, Wester H-J, Weber W, et al. Noninvasive imaging of alpha v beta 3 integrin expression using F-18-labeled RGD-containing glycopeptide and positron emission tomography. *Cancer Res.* 2001;61:1781–1785.
27. Achilefu S, Bloch S, Markiewicz MA, et al. Synergistic effects of light-emitting probes and peptides for targeting and monitoring integrin expression. *Proc Natl Acad Sci U S A.* 2005;102:7976–7981.
28. Haubner R, Wester HJ, Reuning U, et al. Radiolabeled alpha(v)beta3 integrin antagonists: a new class of tracers for tumor targeting. *J Nucl Med.* 1999;40: 1061–1071.
29. Takeshita S, Kaji K, Kudo A. Identification and characterization of the new osteoclast progenitor with macrophage phenotypes being able to differentiate into mature osteoclasts. *J Bone Miner Res.* 2000;15:1477–1488.
30. Kitaura H, Sands MS, Aya K, et al. Marrow stromal cells and osteoclast precursors differentially contribute to TNF-α-induced osteoclastogenesis in vivo. *J Immunol.* 2004;173:4838–4846.
31. Wang M, Caruano AL, Lewis MR, Meyer LA, VanderWaal RP, Anderson CJ. Subcellular localization of radiolabeled somatostatin analogues: implications for targeted radiotherapy of cancer. *Cancer Res.* 2003;63:6864–6869.
32. Qi J, Leahy RM. Resolution and noise properties of MAP reconstruction for fully 3-D PET. *IEEE Trans Med Imaging.* 2000;19:493–506.
33. Ohshima H, Nakasone N, Hashimoto E, Sakai H, Nakakura-Ohshima K, Harada H. The eternal tooth germ is formed at the apical end of continuously growing teeth. *Arch Oral Biol.* 2005;50:153–157.
34. Chen X, Park R, Tohme M, Shahinian AH, Bading JR, Conti PS. MicroPET and autoradiographic imaging of breast cancer alpha v-integrin expression using ^{18}F- and ^{64}Cu-labeled RGD peptide. *Bioconjug Chem.* 2004;15:41–49.
35. Wu Y, Zhang X, Xiong Z, et al. microPET imaging of glioma integrin $\alpha_v\beta_3$ expression using ^{64}Cu-labeled tetrameric RGD peptide. *J Nucl Med.* 2005;46: 1707–1718.
36. Chen X, Liu S, Hou Y, et al. MicroPET imaging of breast cancer alphav-integrin expression with ^{64}Cu-labeled dimeric RGD peptides. *Mol Imaging Biol.* 2004;6: 350–359.
37. Faccio R, Takeshita S, Zallone A, Ross FP, Teitelbaum SL. c-Fms and the $\alpha_v\beta_3$ integrin collaborate during osteoclast differentiation. *J Clin Invest.* 2003;111:749–758.
38. Bazzoni G, Hemler ME. Are changes in integrin affinity and conformation overemphasized? *Trends Biochem Sci.* 1998;23:30–34.
39. Horton MA, Dorey EL, Nesbitt SA, et al. Modulation of vitronectin receptor-mediated osteoclast adhesion by Arg-Gly-Asp peptide analogs: a structure-function analysis. *J Bone Miner Res.* 1993;8:239–247.
40. Sambrook P, Cooper C. Osteoporosis. *Lancet.* 2006;367:2010–2018.
41. Teitelbaum SL. Osteoclasts: culprits in inflammatory osteolysis. *Arthritis Res Ther.* 2006;8:201–208.